

Mechanical, microstructural and fracture properties of dissimilar welds produced by friction stir welding of AZ31B and Al6061



A. Dorbane^{a,c}, B. Mansoor^{a,*}, G. Ayoub^{a,b}, V.C. Shunmugasamy^a, A. Imad^c

^a Mechanical Engineering Program, Texas A&M University at Qatar, Doha, Qatar

^b Department of Mechanical Engineering, American University of Beirut, Beirut, Lebanon

^c Laboratoire de Mécanique de Lille, Ecole Polytech'Lille, University of Lille, Lille, France

ARTICLE INFO

Article history:

Received 18 September 2015

Received in revised form

3 November 2015

Accepted 6 November 2015

Available online 10 November 2015

Keywords:

Friction stir welding

Dissimilar metal joining

Tensile properties

High-temperature properties

Microstructure

ABSTRACT

Friction stir welding (FSW) has been used for joining AZ31B magnesium alloy and Al 6061-T6 aluminum alloy sheets. In this regard, the current work aims to study the mechanical, microstructural and fracture properties of dissimilar FSW welds obtained by evolving the tool rotation and translation speeds. The dissimilar welds microstructure and mechanical properties are evaluated and correlated with the FSW parameters to obtain the optimum weld conditions. The results showed that placing aluminum on the advancing side of the weld resulted in better quality welds. The evaluation of the microhardness along the joint section showed values evolving between the microhardness values of the base metals (Al and Mg). A discontinuity in the microhardness values, attributed to the intermetallic compounds (IMC) present, was observed at the weld interface between Mg and Al sheets. The room temperature tensile testing of the weld showed weld joint efficiency between 18% and 55% and at higher temperatures (200 °C) joint efficiency was observed to be between 58% and 78%. The specimen showed brittle behavior under tensile testing, and the specimen fracture occurred along the weld joint. The specimen fracture seems to have initiated in the brittle Mg_2Al_3 and $Mg_{17}Al_{12}$ IMCs formed between the welded sheets.

© 2015 Elsevier B.V. All rights reserved.

1. Introduction

Utilization of lightweight metals such as magnesium (Mg), aluminum (Al) and titanium (Ti) to form weight saving structural components in aerospace and automotive vehicles can significantly benefit in improving fuel efficiency and reducing harmful emissions [1,2]. The ability to produce components from different lightweight metal alloys and to integrate them together is an important technical challenge. One principal aim is to improve reliable inhomogeneous metal joining methods to enable the production and integration of mechanical components made from lightweight substitute metal alloys.

Magnesium and aluminum are two of the lightest structural metals and joining these two metals presents several challenges. For this, several conventional welding techniques such as gas tungsten arc welding (GTAW) [3,4], electron beam welding (EBW) [4,5], laser beam welding (LBW) [6], have been used to weld Al alloys to Mg alloys. These conventional welding techniques results in coarse-grained and intermetallic (both large and continuous) regions in the weld zone followed by a prominent heat affected

zone (HAZ) and the base material (BM) [7]. Some of the other welding techniques such as brazing based on Zn-based filler materials [8,9], diffusion bonding [10,11], cold metal transfer MIG welding [12,13] and conventional MIG and TIG welding [14–16] have been used. In all of these welding techniques used to weld Al alloy to Mg alloy, solidification of the metal occurs resulting in the formation of intermetallic compounds. The resulting formation of various types of intermetallic compounds (IMC) in the weld zone undermines the weld integrity. Also, controllability of the distribution, size and type of the brittle IMCs are difficult, and their presence has a detrimental effect on the weld strength.

To obtain defect free joining of dissimilar metals Al and Mg, studies have utilized solid state welding techniques such as ultrasonic welding [17,18], resistance spot welding [19], linear friction welding [20], and friction stir welding (FSW) [21–30]. The advantage with the solid state welding technique is that it offers controllability over heat generation and response times. To capitalize this benefit, a solid state metal joining technique, namely FSW that utilizes frictional heat, metal mixing and severe plastic deformation caused by a rotating shouldered tool with a pin and the metal to be welded, has been widely used [31]. The tool rotation results in stirring and plastic deformation of the metals at high temperature, which results in a joint with good weld integrity. The FSW process takes place below the melting

* Corresponding author.

E-mail address: bilal.mansoor@qatar.tamu.edu (B. Mansoor).

Table 1
Summary of existing literature studies on dissimilar FSW on Al6061–AZ31 alloys.

Study	Tool properties	Weld parameters	Outcome
[49] Al6061 (both metals on either side)	Shoulder dia.: 10 mm, Pin diameter: 4 mm, Pin length: 1.3 mm (Butt joint) Pin length: 1.5 mm (Lap joint) H13 tool steel, concave shoulder and threaded pin	Butt joint Rotation – 800 and 1400 rpm Tool tilt – 3° Travel speed – 38 mm/min Tool Offset – 1.5 mm (Al and Mg) Lap joint Rotation – 800 and 1400 rpm Tool tilt – 3° Travel speed – 38 mm/min Tool Offset – 1.5 mm (Al and Mg)	1. In butt welding higher strength was observed with mg on the advancing side. 2. Tool offset towards Mg side resulted in improved joint strength.
[28] Al6061-T6 (both metals on either side)	Shoulder dia.: 10 mm, Pin diameter: 4 mm, Pin length: 1.3 mm (Butt joint) H13 tool steel, concave shoulder and threaded pin	Butt joint Rotation – 1000–2200 rpm Tool tilt – 3° Travel speed – 38–305 mm/min. Tool Offset – 1.5 mm (Al and Mg)	1. The average peak temperature attained decreased with increasing tool travel speed. 2. Under identical welding conditions, the average peak temperature measured is higher when Al is placed on the advancing side.
[37] Al6061-T6 (AS for butt weld)	Shoulder dia.: 10 mm, Pin diameter: 4 mm, Pin length: 1.3 mm (Butt joint) H13 tool steel, concave shoulder and threaded pin Shoulder dia.: 10 mm, Pin diameter: 4 mm, Pin length: 1.5 and 2.3 mm H13 tool steel, concave shoulder and threaded pin	Butt joint Rotation –1400 and 2200 rpm Tool tilt – 3° Travel speed – 38 and 254 mm/min Tool Offset – 1.5 mm (Al and Mg) Lap joint Rotation –1400 and 2200 rpm Tool tilt – 3° Travel speed – 38 and 254 mm/min Tool Offset – 1.5 mm (Al and Mg)	1. In lap welding, the IMCs observed on the Al side of the weld was identified as Al ₃ Mg ₂ and on the Mg side, was identified as an eutectic consisting of Al ₁₂ Mg ₁₇ . 2. The liquid formation during the FSW process was evidenced by the presence of Mg ₁₇ Al ₁₂ and Mg in the stir zones of the butt and lap welds.
[29] AA6061 (both metals on either side)	Shoulder dia.: 12–24 mm, Pin diameter: 5–6 mm, Pin length: 5.7 mm (Butt joint) HSS tool material, tapered pin	Butt joint Rotation –400 rpm Tool tilt – 0° Travel speed – 19.8 mm/min Axial force – 12 kN	1. Effect of tool shoulder diameter on the weld properties is studied. 2. Joint prepared with 21 mm shoulder diameter showed 192 MPa tensile strength and 89% joint efficiency in comparison to Mg alloy.
[40] 6061-T6 (both metals on either side)	Shoulder dia.: 10 mm, Pin diameter: 3.2 mm, Pin length: 2.8 mm (Butt joint) H13 tool steel, concave shoulder and frustum-shaped right-hand threaded pin.	Butt joint Rotation – 500–1000 rpm Tool tilt – 3° Travel speed – 30–80 mm/min Tool Offset – 0–0.6 mm Plunge depth – 0.12 mm	1. Mg on the AS resulted in higher tensile strength (140 MPa), than Al on the AS, at a tool offset of 0.3 mm. 2. The highest tensile strength (175 MPa) was observed for 700 rpm, 50 mm/min, Mg on AS and tool offsetted to 0.3 mm towards Mg.
[41] Al6061 (AS)	Shoulder dia.: 15 mm, Pin diameter: 3 mm, Pin length: 2.9 mm (Butt joint) H13 tool steel, concave shoulder	Butt joint Rotation –600–1400 rpm Tool tilt – 2.5° Travel speed – 20–60 mm/min Tool Offset – 0–0.6 mm	1. Defect free weld was attained for a tool rotational speed of 1000 rpm/min and translational speed of 40 mm/min, for the used tool geometry. 2. Tensile strength of the welded joint was 76% and 60% of Mg AZ31 and Al6061 alloys, respectively.
[50] Al6061 – T6 (RS)	SKD61 tool steel, concave shoulder and truncated cone type pin, coated with AlTiN	Butt joint Rotation – 1200 rpm Tool tilt – 2° Travel speed – 20–101.6 mm/min Tool Offset – 0.1 mm (towards Mg)	1. Average grain size of 2.5 and 4.5 μm was observed on the Al and Mg stir zones, respectively. This is very small in comparison to 28 and 15 μm observed on the corresponding BM. 2. The interface microstructure comprised of lamellar like shear bands rich in Al or Mg.

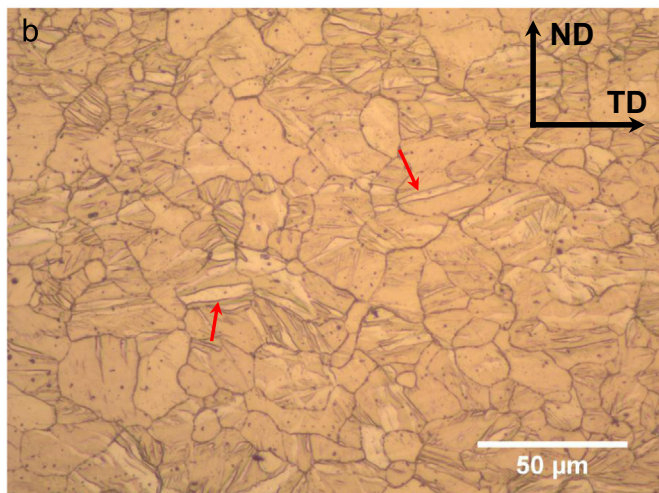
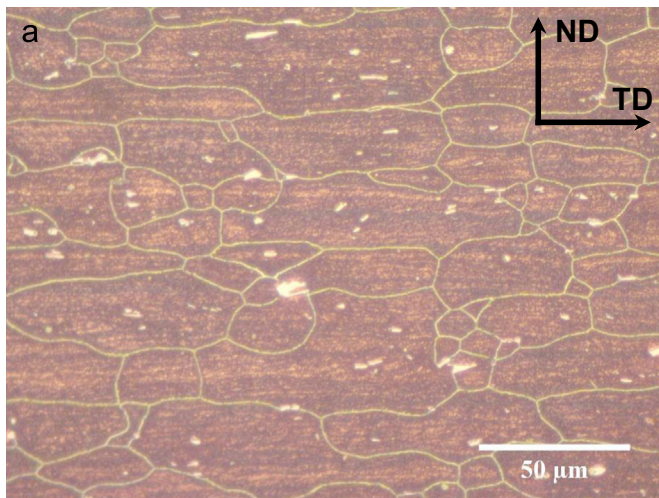
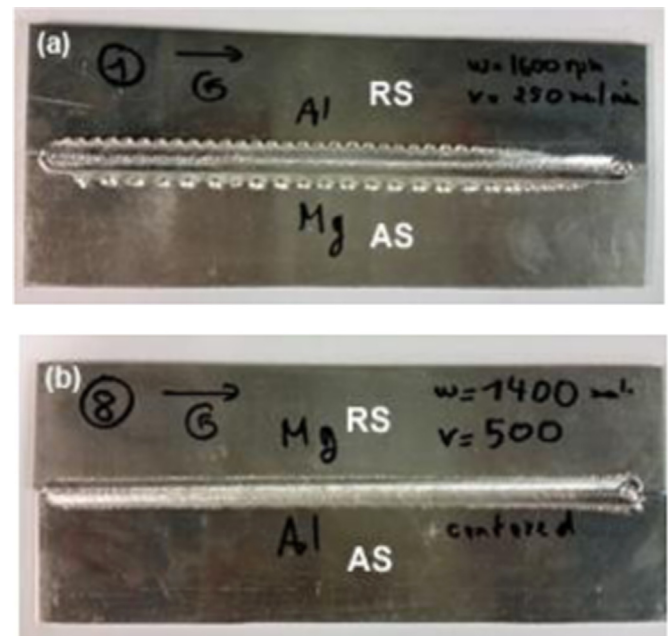
Table 1 (continued)

Study	Tool properties	Weld parameters	Outcome
[51]	Shoulder dia.: 19 mm, Pin diameter: 5 mm,	Rotation –800 rpm Travel speed – 90 mm/ min Tool Offset – 75% tool towards AS. Double sided weld.	1. Approximately three times the Vickers Hardness is observed in the stir zone, which is attributed to the complex vortexes and lamellar structure found in the SZ. 2. Dynamic recrystallization was observed in the weld zone and the transition zone which resulted in reduced grain size in the SZ in comparison to the BM.

Table 2

The nominal composition along with mechanical properties of Al and Mg alloys used in present study.

Alloy	Wt%	Al	Mn	Mg	Si	Cu	Cr	Fe	Zn	Ti	Ca	Ni	YS (MPa)	UTS (MPa)
Al6061-T6	Min	Bal	–	0.8	0.4	0.15	0.04	–	–	–	–	–	275	350
	Max	Bal	0.15	1.2	0.8	0.4	0.35	0.7	0.25	0.15	–	–		
AZ31B	Min	2.5	0.2	Bal	–	–	–	–	0.6	–	–	–	150	300
	Max	3.5	1	Bal	0.1	0.05	–	0.005	1.4	–	0.04	0.005		

**Fig. 1.** Microstructure of the base materials (a) Al 6061-T6 and (b) AZ31B.**Fig. 2.** Al–Mg FS welded specimens (a) 1600 rpm, 250 mm/min, Mg on the AS and (b): 1400 rpm, 500 mm/min, Al on the AS [34].

temperature of the alloy, so several defects due to the solidification of the metals are avoided [32].

Studies in existing literature have utilized FSW to weld dissimilar alloys of magnesium and aluminum alloys and have studied the weld microstructure and mechanical properties such as micro-hardness and tensile properties. The studies on dissimilar FSW of Mg AZ31 alloy with Al6061 alloy is summarized in Table 1.

The tool properties, weld parameters and the outcomes from the studies has been summarized in the table. Most of the studies on the existing literature have concentrated on optimizing process parameters based on the weld microstructure. Only a few studies are available on the mechanical properties of the weld. Also temperature effects on the tensile properties of dissimilar Al/Mg joints have not been investigated in the existing literature. Considering that the welded joints used in the automotive, aerospace and oil and gas industries will be subjected to temperature changes during their service life, understanding the properties of the joints at elevated temperature is important. This study attempts to characterize the FS welded joints at high temperature as well as at room temperature, to better understand the behavior of the welded joints, compared with the base material. In this regard the study has focused on the effect of process parameters on the weld zone microstructure and its subsequent impact on room temperature (25 °C) and high temperature (200 °C) mechanical and fracture properties.

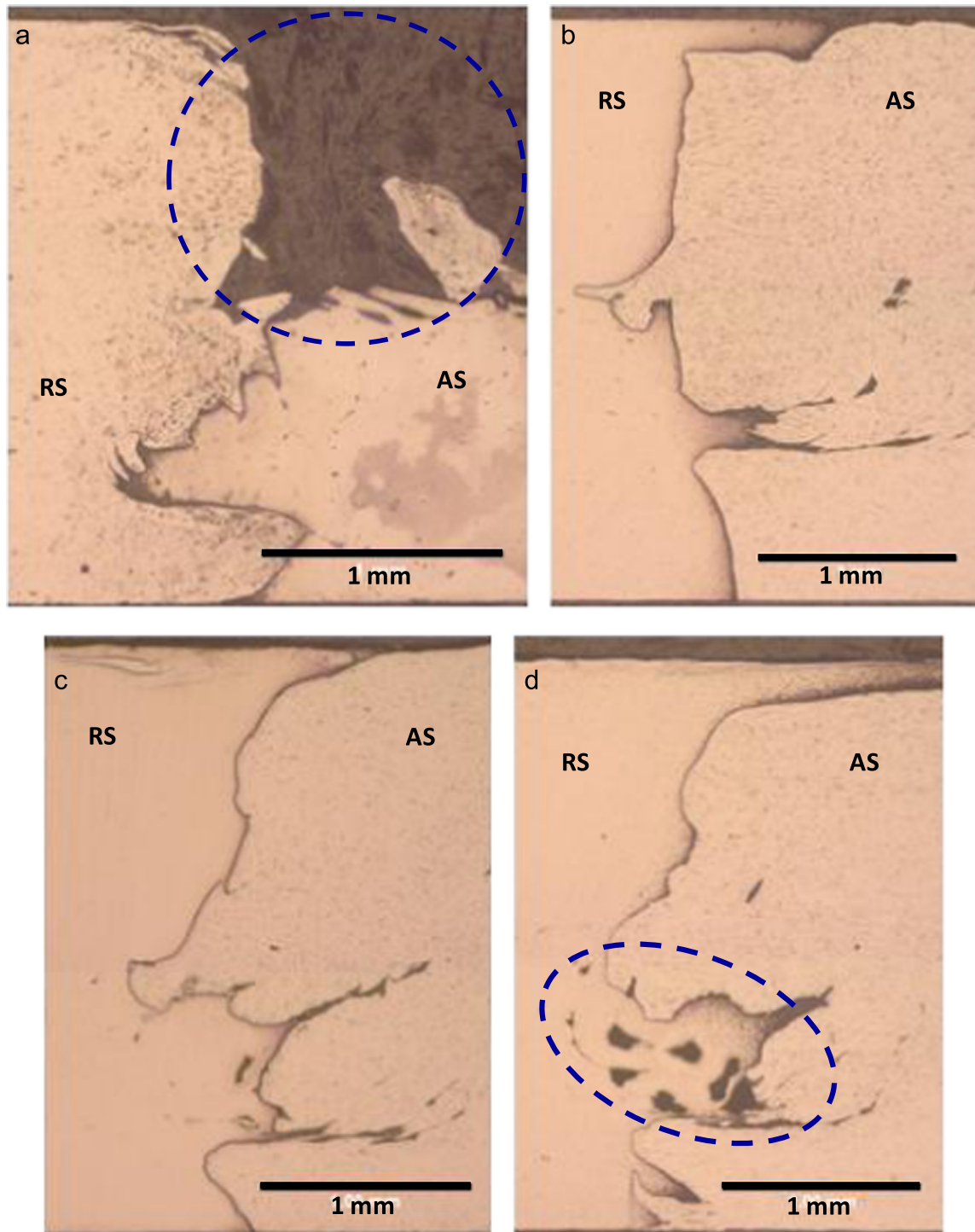


Fig. 3. Optical microscope observation of the cross section of the welded joint obtained using parameters (a) 1600 rpm rotational and 250 mm/min translational speeds (Al on the RS). (b–d) Fixed translational speed of 500 mm/min with variable rotational speeds of 1600, 1400, 1200 rpm, respectively with aluminum on the AS [34].

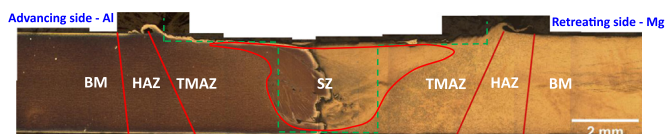


Fig. 4. Cross section of Al/Mg weld prepared utilizing 1400 rpm and 500 mm/min weld parameters, showing the various zones on the weld.

2. Experimental procedure

In the present work, the FSW operation was carried out using a Gantry FSW Machine (FSW-LM-08, Beijing FSW Tech. Co. Ltd.). The tool utilized to join Al/Mg had a tool shoulder diameter of 10 mm with a threaded pin of length 2.96 mm. The maximum and minimum diameters of the threaded pin are 3.6 mm and 2.9 mm,

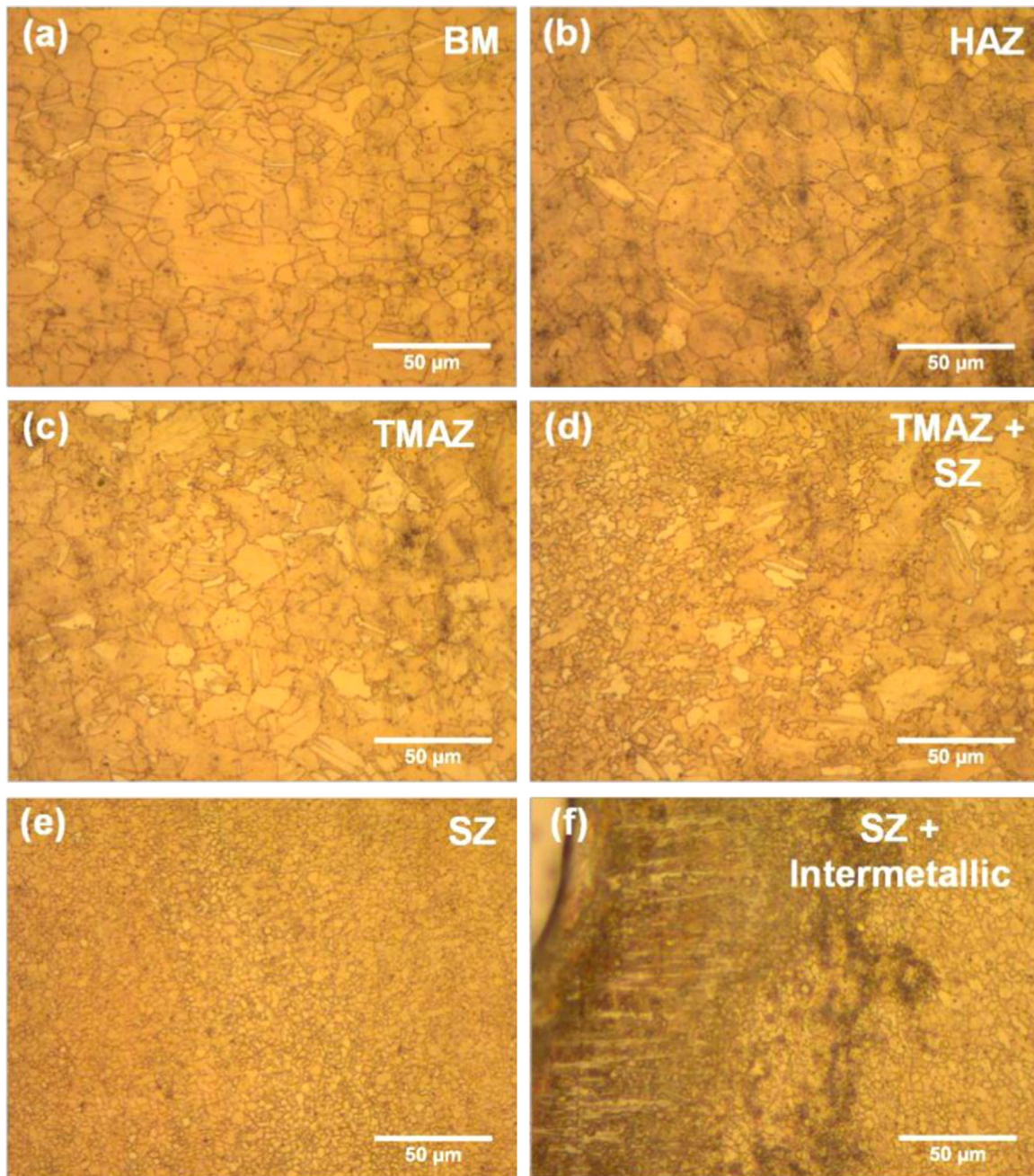


Fig. 5. Microstructure of the different zones on the magnesium side of the FS welded dissimilar Al–Mg joint prepared using 1400 rpm and 500 mm/min [34].

respectively. All the FSW runs were performed with a tool tilt angle of 3° . The Al and Mg plates to be FS welded were $250 \times 50 \times 3 \text{ mm}^3$ in dimensions and were cut from the base material. The plate edges were deburred to prevent any prior inhomogeneities. A deburring tool was used to remove the cut plate edges and to ensure a smooth welding between the plates. The used base materials are Al6061-T6 aluminum and AZ31B magnesium; obtained from commercial suppliers and their nominal chemical composition are presented in Table 2. Prior to the microstructural examination on the base material and welded joint specimens the mounted specimens were grounded and polished up to 1200 grit followed by $1 \mu\text{m}$ diamond slurry and $0.04 \mu\text{m}$ colloidal silica. To observe the microstructural features, the Mg and the Al parts of the weld were etched using standard acetic-picric solution (4.2 g picric acid, 10 ml acetic acid, 70 ml ethanol and 10 ml distilled water) and Weck's reagent (4% KMnO_4 and 1% NaOH diluted in distilled water), respectively [33].

An optical (light) microscope (Zeiss AxioVert 40 MAT fitted with ERc5s camera) and a scanning electron microscope (SEM) were used to observe microstructure, intermetallics and different zones formed after the weld. The welded specimens were evaluated for Vickers micro-hardness using parameters of 100 gf and dwell time of 15 s. The microhardness measurements were performed at 2 mm from the top of the weld in the thickness plane (normal direction–transverse direction (ND–TD) plane, perpendicular to the welding direction). The hardness values were also measured at three different distances from the top of the weld to study the variation of the hardness in the welded joint. ASTM E8/E8M-15 (ASTM International, PA, USA) tensile test specimen geometry was used for the tensile experiments. Uniaxial tensile tests were performed at room temperature and $200 \pm 3^\circ\text{C}$ under constant strain rate of 10^{-3} s^{-1} , using a computer controlled MTS insight tensile testing machine equipped with a 30 kN load cell and equipped with a LBO-series Thermocraft LabTemp laboratory

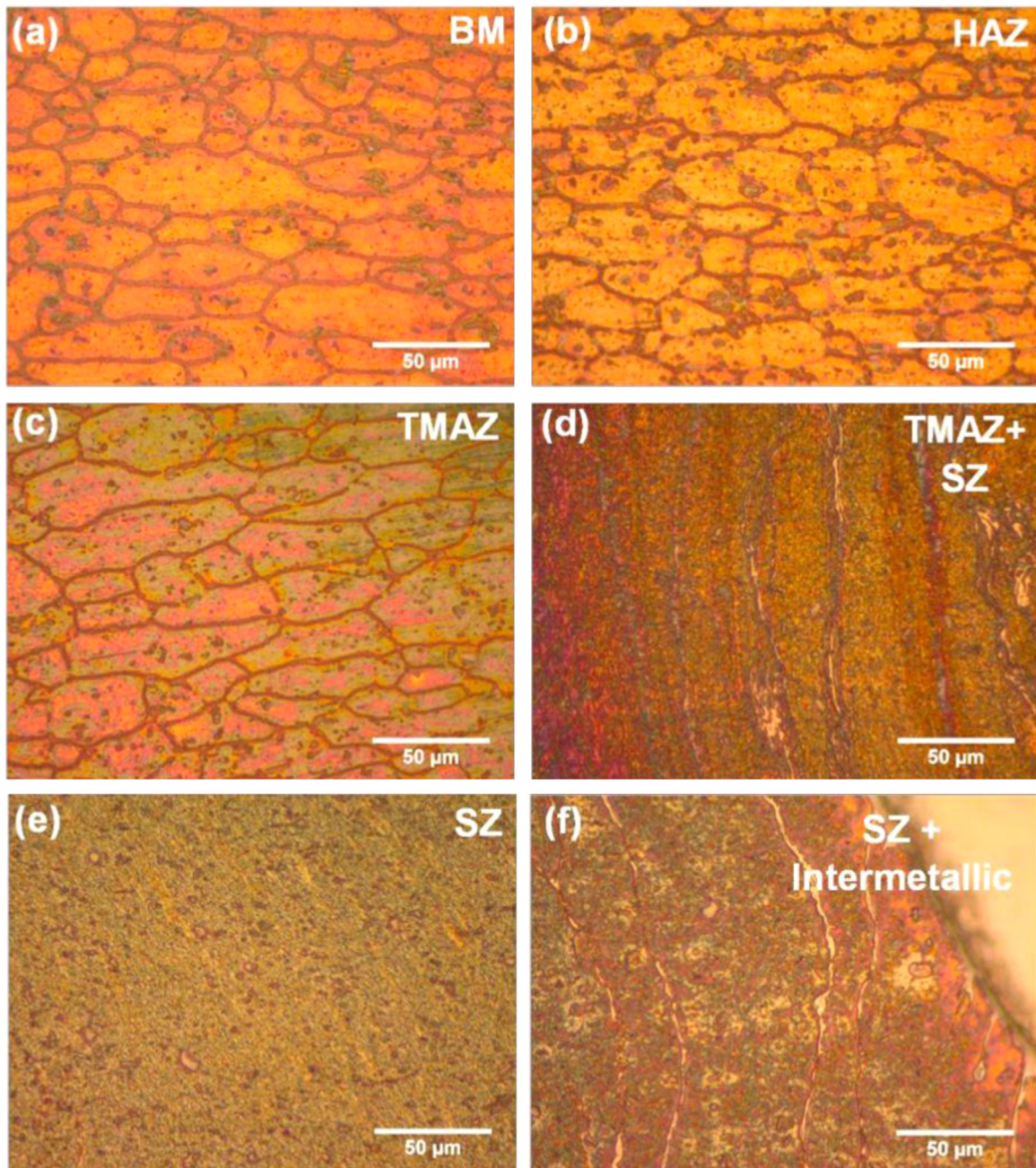


Fig. 6. Microstructure of the different zones on the aluminum side of the FSW welded dissimilar Al–Mg joint prepared using 1400 rpm and 500 mm/min.

oven (environmental chamber). For the high-temperature tensile testing, specimens were kept inside the environmental chamber for 5 min to homogenize the temperature, prior to starting the tensile experiment. SEM observations of the thickness plane of the welded Al and Mg plates and the fractured tensile tested specimens were performed.

3. Results and discussion

3.1. Macro and microstructure

3.1.1. Base material

The investigated base materials are Al 6061-T6 (rolled sheets 3 mm thick supplied by McMaster Inc.) and magnesium AZ31B (twin rolled cast rolled 3 mm thick supplied by POSCO (Seoul,

Korea). Fig. 1(a) and (b) represents the microstructure of the base materials (BM) (Al6061-T6 and AZ31B) used in the present study. Both microstructures are observed in the ND–TD plane. The grains of the Al6061-T6 have the shape of elongated ellipses, and the iron-rich phases and the magnesium silicide particles scattered throughout the microstructure are clearly observed [33]. The microstructure of the magnesium base metal reveals mainly equiaxed grained and some twins can be observed which are most probably due to the rolling conditions. Grain size analysis was performed on the BMs–Al and Mg showed an average grain size of $20.52 \pm 11.95 \mu\text{m}$ and $11.46 \pm 4.59 \mu\text{m}$, respectively. The obtained microstructure of the BMs is helpful for comparison with the different observed weld zones.

3.1.2. FSW joint – macrostructure

Fig. 2(a) and (b) represents the images of two welded specimens. Fig. 2(a) shows the dissimilar weld of Al and Mg carried out

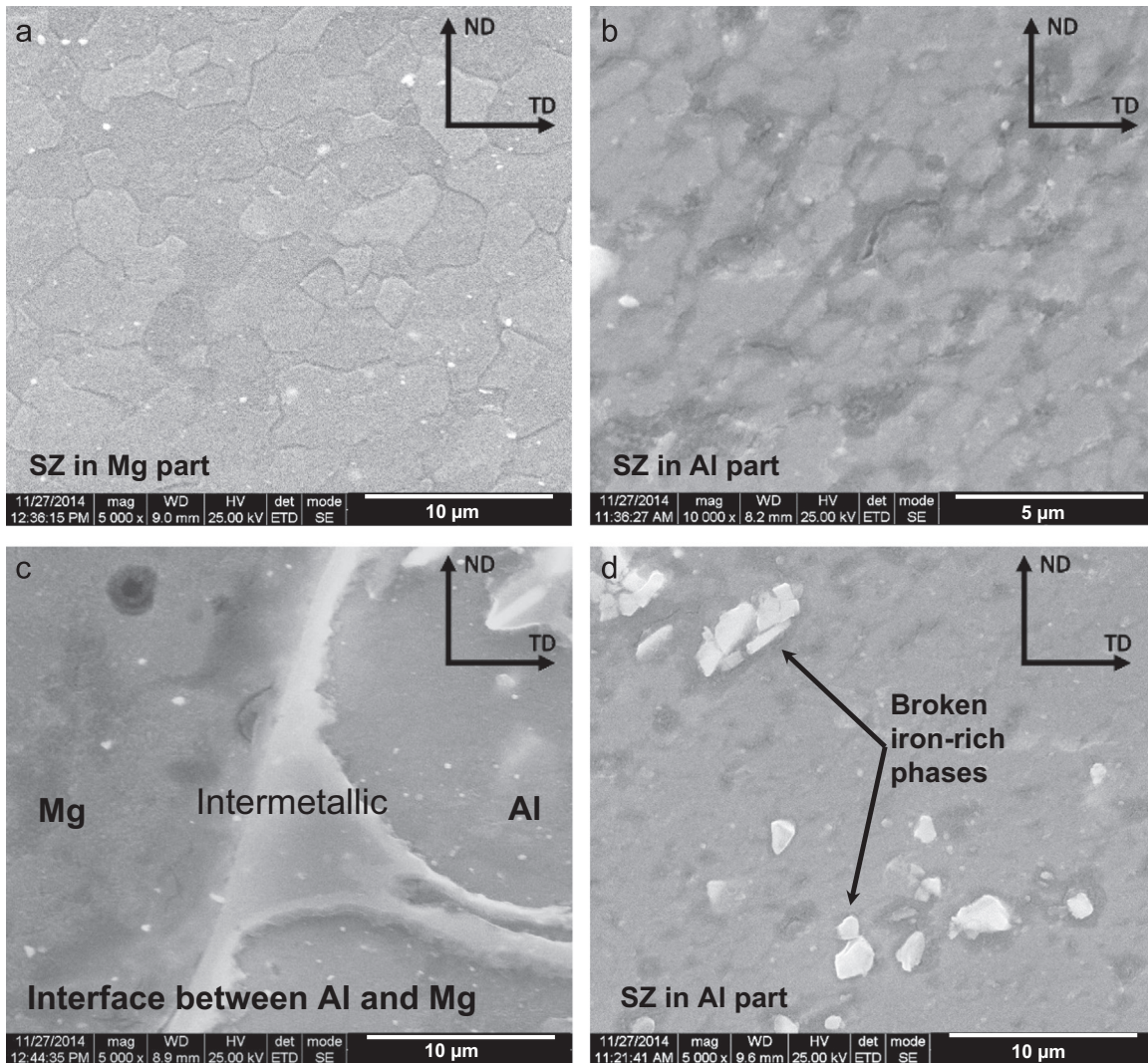


Fig. 7. SEM analysis of the SZ in the joint prepared using 1400 rpm and 500 mm/min. (a) magnesium stir zone, (b) aluminum stir zone, (c) Intermetallic in the Al/Mg interface and (d) aluminum stir zone showing broken precipitates.

using tool rotational speed of 1600 rpm and translation speed of 250 mm/min with placing Mg on the advancing side (AS). While Fig. 2(b) presents, the visual aspect of FS welded plates employing 1400 rpm and 500 mm/min weld parameters with Al on the AS. From Fig. 2 it could be observed that irrespective of the different welding parameters used for the two cases, the placement of Al has a significant effect on the weld integrity. Placing Al plates on the AS of the joint resulted in a defect-free weld as could be observed in Fig. 2(b). This observation was further validated by examining the weld zone under an optical microscope for the different welding parameters, with Al or Mg plates placed in AS. The obtained weld cross-sections optical microscope images (in ND–TD plane) were utilized to differentiate the two welded materials Al (6061-T6), and Mg (AZ31B) and to observe the weld defects. Fig. 3 presents optical microscope images of the heterogeneous FS welded Al–Mg joints, obtained with different Al plate configurations and welding parameters. As a general observation; good welds are obtained by placing aluminum on the AS, confirming the observations in Fig. 2. Placing aluminum on the Retreating Side (RS) resulted in defects such as voids and surface galling in the weld as can be seen in Fig. 3(a). Similar results with the placement of Al in the welding plate configuration, has been observed in literature studies and in the pilot work to this study, on dissimilar FSW of Al alloys to Mg alloys [21–30,34]. The weld microstructure

was observed by varying the tool rotation speed from 1200 rpm to 1600 rpm with the translation speed being kept at a constant speed of 500 mm/min. The microstructure corresponding to the welds using tool rotation speed of 1600, 1400 and 1200 rpm are shown in Fig. 3(b)–(d), respectively. From these images it is observed that the welds with aluminum on the AS had fewer defects (Fig. 3(b, c)), in comparison to aluminum on the RS (Fig. 3(a)). Comparing Fig. 3(b)–(d), some defects such as wormhole and voids are observed on the Mg side with the most evident defects detected in the 1200 rpm rotation speed specimen, in comparison to the other two rotation speeds. While analyzing the microstructures, the plate welded with aluminum placed in the AS with a rotation speed of 1400 rpm and translation speed of 500 mm/min presented the best observable weld quality.

3.1.3. FSW joint – microstructure

The complete structure of the dissimilar Al–Mg friction stir welded joint cross-section (ND–TD plane) obtained with 1400 rpm and 500 mm/min weld parameters is shown in Fig. 4. This figure displays the extent of the different zones constituting the cross-sectional microstructure namely base material (BM), heat affected zone (HAZ), thermo-mechanically affected zone (TMAZ) and stir zone (SZ) on both the magnesium and aluminum sides of the weld. A detailed microstructure analysis was carried out to study the

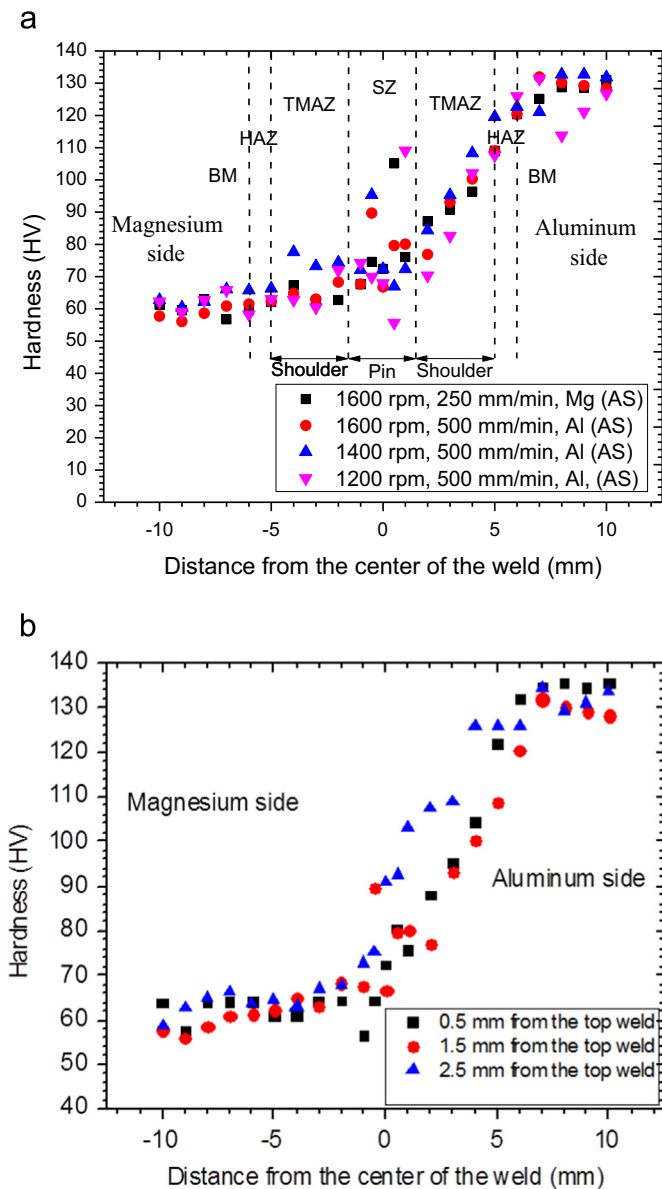


Fig. 8. (a) Micro-hardness values obtained at 2 mm from top of weld for the various parameters studied, namely (1) 1600 rpm, 250 mm/min, (Mg on AS); (2) 1600 rpm, 500 mm/min, (Al on AS); (3) 1400 rpm, 500 mm/min, (Al on AS); (4) 1200 rpm, 500 mm/min, (Al on AS) and (b) Micro-hardness obtained on weld prepared using 1400 rpm, 500 mm/min parameters, at three different distances from top of the weld.

grain size, grain boundaries, and intermetallic zone. The different zones of the weld cross-section (Fig. 4) in the magnesium side and the aluminum side are represented in Figs. 5 and 6, respectively. Distinguishable microstructure can be observed in the four zones of each side of the joint.

The stir zone presents a considerable grain refinement when compared with the base material. On the magnesium side of the weld, the grain size in the SZ was $2.43 \pm 0.87 \mu\text{m}$, in comparison to $11.46 \pm 4.59 \mu\text{m}$ in the base material. On the aluminum side, the grain size reduced from $20.52 \pm 11.95 \mu\text{m}$ in the base material to $0.94 \pm 0.24 \mu\text{m}$ in the SZ. The grain refinement obtained in the dissimilar FSW of Al–Mg alloys is corroborated with the results previously reported in existing literature on dissimilar FSW of Al–Mg alloys [21–30]. The grain refinement can be correlated to the severe deformation encountered by the aluminum and magnesium in the SZ and also with the heat input that was not enough to induce grain growth. The prediction of grain size resulting from

friction stir processing was investigated as a function of the strain rate, the process induced temperature and the materials properties [35,36]. However using these models to predict the grain size with dissimilar FSW can be challenging. In the magnesium side, the TMAZ shows a larger number of twins compared to the BM with an average grain size equal to $8.44 \pm 4.10 \mu\text{m}$. The HAZ shows larger grains with an average size equal to $14.75 \pm 5.60 \mu\text{m}$ and fewer twins are perceptible. In the aluminum side, the TMAZ is characterized with more elongated and bigger grains compared to the BM, with an average grain size of $21.16 \pm 10.70 \mu\text{m}$. Much bigger grains are observable in the HAZ, with a mean grain size equal to $26.15 \pm 8.78 \mu\text{m}$.

3.1.4. Scanning electron microscopy observations

Fig. 7 shows SEM micrographs observation of the SZ of Al/Mg dissimilar welded sheet joined using 1400 rpm and 500 mm/min weld parameters placing aluminum on the AS. Fig. 7(a) and (b) reveals an equiaxed microstructure of the SZ in Mg and Al sides, respectively. The microstructure of the SZ seems to be the consequence of a completely recrystallization that resulted in a very fine grains structure. It can be assumed that the observed microstructure resulted from a severe deformation with not enough heat input to induce a sizeable grain growth. Fig. 7(c) shows the interface between Mg and Al separated by a thin layer of IMC. Friction stir welding of aluminum and magnesium results in the formation of brittle IMCs such as Mg_2Al_3 and $\text{Mg}_{17}\text{Al}_{12}$. The formation of IMC was reported to occur in localized fusion zones, which is strongly dependent on the heat input resulting from the weld parameters. Therefore, the IMCs are most likely to form in weld zone that encountered the highest temperature, more precisely at the interface between aluminum and magnesium and in some localized areas of the SZ. A higher percent of IMCs has been reported in the SZ compared to the BMs [22,27,29,37–41]. Fig. 7(d) shows broken precipitates present in the Al part of the stirred zone, probably induced by the severe deformation encountered by the material during FSW [33]. The SEM images present a defect-free interface between the FS welded Al6061-T6 and AZ31B alloys. The microstructure and the weld integrity analysis demonstrated that 1400 rpm rotational speed and 500 mm/min translational speed can be used as the optimum welding parameters in the present study. The optimum parameters observed in the study are based on the tool geometry used. The analysis of the microstructure revealed a defect free weld with the presence of brittle IMCs in the SZ. Observable IMC layer at the interface between magnesium and aluminum suggested that the interface reached a high temperature close to melting during the FSW process. Also, the presence of IMCs at the interface suggests that the most probable zone of crack initiation during mechanical loading will be the interface between the magnesium and aluminum.

3.2. Micro-hardness testing

The magnesium crystalline structure is a hexagonal-closed pack (HCP), the crystal unit cell of aluminum is face-centered cubic (FCC), $\text{Mg}_{17}\text{Al}_{12}$ has a body-centered cubic (BCC) crystal structure and finally the Mg_2Al_3 intermetallic phase has a Fd-3m structure [42]. The different crystalline structures composing the SZ induce a high level of incoherency at the interfaces between the various constituents. In order to detect the difference in the mechanical and microstructural properties of the different zones of the weld and in the purpose of identifying the zones of the welds where fracture is most probable to occur micro-hardness testing was conducted.

The weld parameters analyzed with the microhardness were 1600 rpm, 250 mm/min, (Mg on AS); 1600 rpm, 500 mm/min, (Al on AS); 1400 rpm, 500 mm/min, (Al on AS); 1200 rpm,

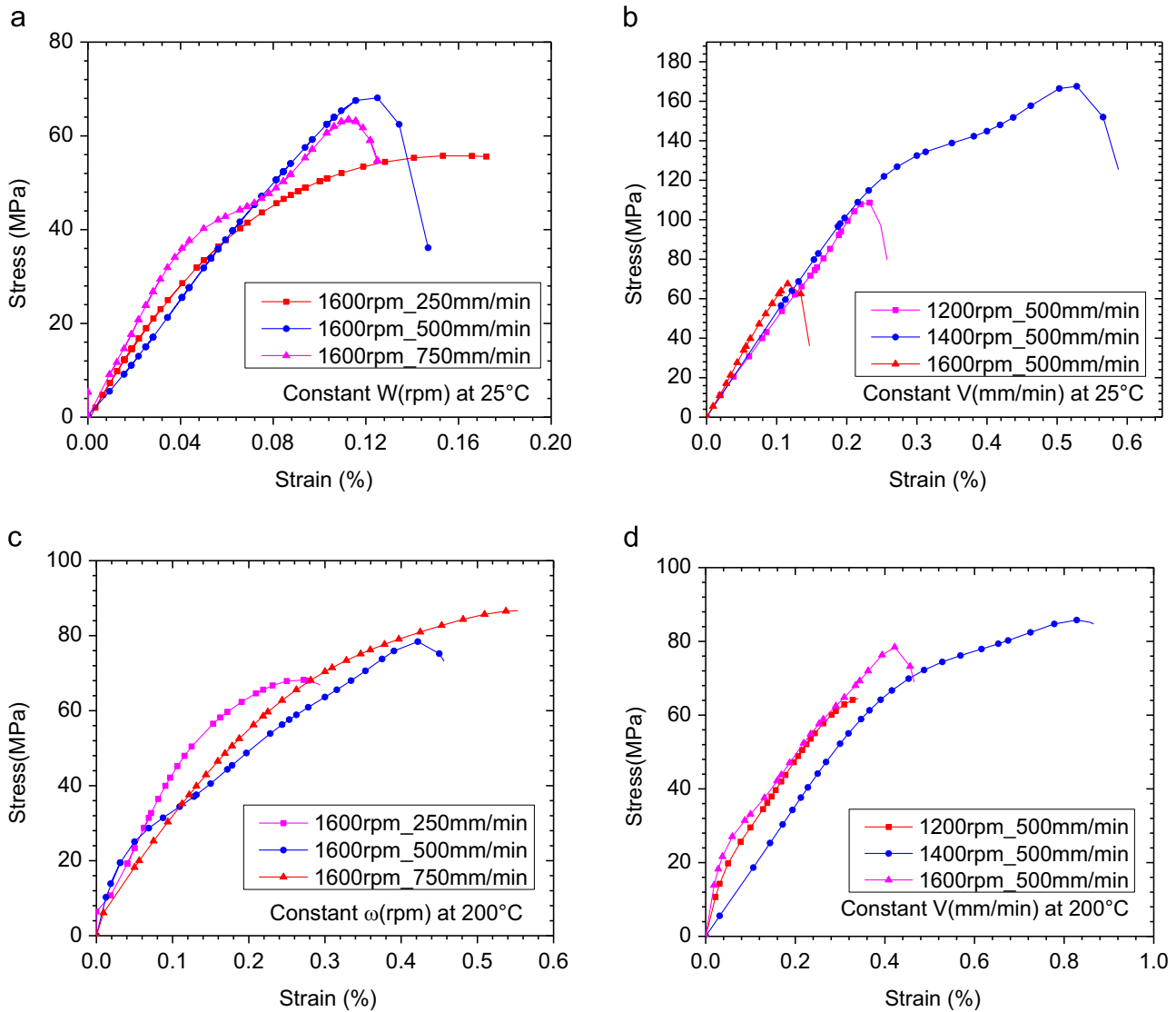


Fig. 9. Engineering stress–strain curves of uniaxial tensile tested welds at room temperature and 10^{-3} s^{-1} with (a) constant tool rotation speed, (b) constant tool translation speed, and at 200°C with (c) constant tool rotation speed and (d) at constant tool translation speed.

500 mm/min, (Al on AS) and the results are shown in Fig. 8. The hardness on the magnesium side (BM) of the weld was found to be between 55 HV and 65 HV and on the aluminum side (BM) was between 120 HV and 135 HV. Fig. 8(a) shows the evolution of hardness values of the investigated samples. The measurements were conducted at the centerline of the weld between -10 and 10 mm on either side of the weld center in which -5 to 5 mm on either side of the weld center corresponds to the tool shoulder diameter. A transition in the hardness values can be observed between the Mg to the Al side. The region corresponding to the tool pin diameter (-1.5 to 1.5 mm on either side of the weld center) shows peaks in the hardness values that can be related to the finer grain structure exhibited by the SZ in addition to the presence of the intermetallic phases. Zhang et al. (2010) reported that the microhardness value of the intermetallic phases is much greater than the magnesium BM [43]. Grain boundaries resist the occurrence of deformation hence large grain boundary will result in higher yield stress. A much smaller average grain size was obtained in the SZ compared to the BM as reported in the previous section. As a result, the SZ consists of larger grain boundaries compared to the BM and the other weld zones. Therefore, a higher hardness values can be expected. Furthermore, we can observe

that the change in hardness values from the BM to the SZ is steeper on the Al side compared to the Mg side. This variation in the hardness rate can be explained by the grain size reduction between the BM and the SZ in the Al and the Mg sides. In fact, the grain size of SZ in the Al side reduced to reach 5% of the grain size of the BM, however, the grain size of the SZ in the Mg side reached 21% of the grain size of the BM.

The hardness values at three different distances from the top of the weld are shown in Fig. 8(b) for the 1400 rpm, 500 mm/min (Al on AS) weld parameters. The hardness values are consistent for the three distances, suggesting good weld integrity. Similar to the previous observation a peak of hardness is measured in the SZ, and it appears corresponding to the micro-hardness of the interface between the Al and Mg sides. The 2.5 mm micro-hardness curve shows highest values in Al side compared to the two other micro-hardness curves, which can be associated with a higher percentage of the intermetallic compounds. Fig. 4 shows that the region of the SZ matching with the 2.5 mm micro-hardness line in the Al side has a slightly different color compared to the other region of the SZ in the Al side. Furthermore, [44,45] reported through simulation that a peak of heat flux, strain rate, and flow stress was obtained around the pin tip, and more precisely on the advancing

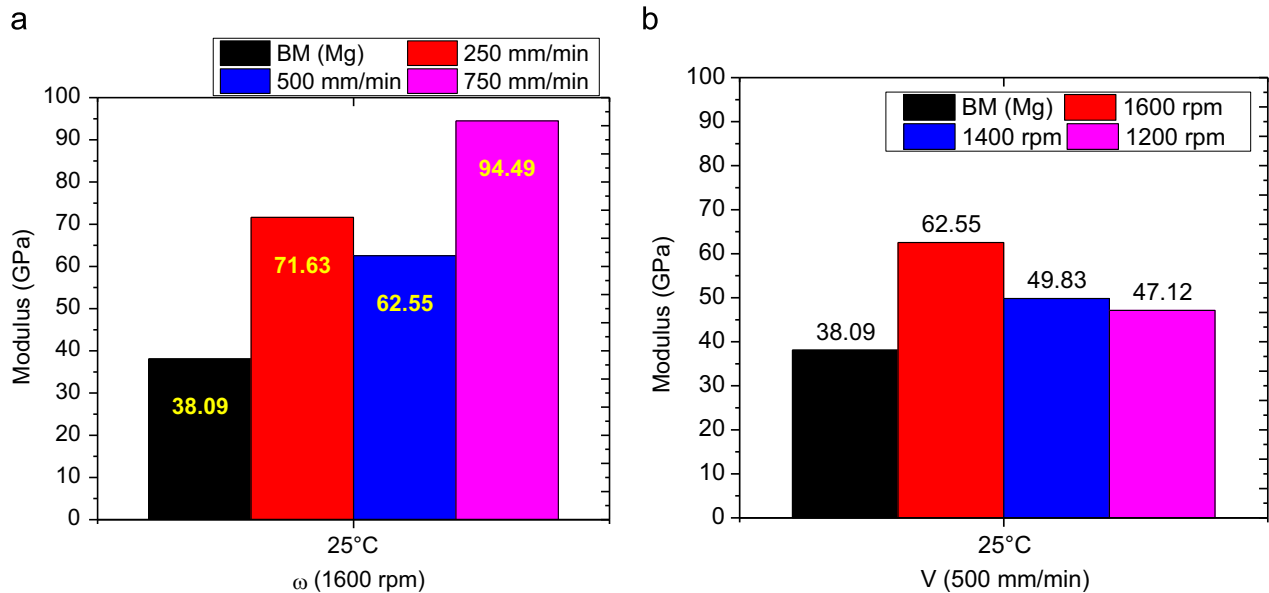


Fig. 10. Modulus calculated at different tool rotation speed and tool translation speed, (a): at constant tool rotation speed (1600 rpm) and (b): at constant tool translation speed (500 mm/min).

side. The formation of IMCs is related to the heat generation during the FSW process [22,37–40]. Therefore, we can assume that this change in color is affected by the change in the composition of this part; hence we assume a higher percentage of IMCs.

Although aluminum and magnesium have different hardness, continuity in the evolution of the hardness was measured by scanning with the micro-indenter the weld region between the two BMs. However, a peak in the hardness values was found at the interface between the aluminum and the magnesium. The peak in the hardness values between the aluminum and the magnesium can be related to an abrupt change in the microstructure, more precisely the grain size and also to the presence of the IMCs (as reported previously in Section 3.1). As the interface between the aluminum and the magnesium is formed by the IMCs, we assume that a higher level of incoherency will induce higher accumulation of dislocations during deformation. Therefore, the process of crack initiation will be further accelerated when the weld is subjected to tensile loading conditions owing to his higher density of dislocations.

3.3. Uniaxial tensile testing

In the purpose of studying the joint efficiency of different weld parameters, to account for potential ranges of operation conditions and finally to study the failure mechanisms; the mechanical response of tensile tests conducted at room temperature and 200 °C at strain rate of 10^{-3} s^{-1} are presented in Fig. 9.

3.3.1. Room temperature

The engineering stress–strain tensile response of dissimilar FSW of Al (on AS) and Mg using constant tool rotation speed of 1600 rpm, and tool translation speeds of 250, 500 and 750 mm/min are presented in Fig. 9(a). From this figure it could be observed that decreasing the translation speed resulted in higher strain to failure but lower strength. This observation can be explained by the fact that reducing the tool translation speed leads to an increase in the heat input, which consequently increase the average grain size resulting in higher strain to failure and lower strength. The stress–strain response of the joint obtained using 750 mm/min as translation speed presented the lowest strain to

failure, which can be the consequence of the less heat input that results into smaller grain size [45–48].

The mechanical response of joints obtained by fixing the tool translational speed at 500 mm/min, and varying the tool rotational speeds between 1200 rpm and 1600 rpm (with Al on AS) are plotted in Fig. 9(b). From this figure, it can be observed that the joint obtained with 1600 rpm tool rotation speed presented the lowest strain to failure and strength compared to the other welding parameters. It was also observed that the joints obtained using 1400 rpm tool rotation speed showed the highest strain to failure. Those observations can be explained by the fact that using 500 mm/min and 1400 rpm as weld parameters produced the optimum heat generation and strain rate which resulted in defect-free joint and higher mechanical properties. The optimum weld parameters found through the current study are associated with the choice of the tool geometry, as heat generation, and the strain rate during welding is strongly dependent on the tool geometry.

The stress–strain response of the studied dissimilar Al/Mg welds exhibited a brittle behavior. In the purpose of analyzing the mechanical properties of the welds, the modulus of the dissimilar welds was calculated in the initial elastic region and compared to the Young's modulus of the AZ31B magnesium alloy (BM). Fig. 10 (a) presents the modulus of magnesium (BM) compared to dissimilar welded Al/Mg joints obtained using constant tool rotational speed of (1600 rpm). The modulus of the BM (Mg) was observed to be 38.09 GPa. The welded specimens yielded to higher modulus with values equal approximately to 1.6–2.5 times the BM's modulus for varying tool translation speeds. It can also be reported from Fig. 10(b) that the modulus was increased by 1.2–1.6 times the BM's modulus for joints obtained at constant tool translation speed of 500 mm/min and by increasing the tool rotational speed. The increase in the modulus values can be explained by the formation of intermetallics that contributes to increasing the resistance to deformation [39,41].

To analyze and compare the mechanical properties of the studied welds, the joint efficiency of the welds was evaluated by normalizing the ultimate tensile strength (UTS) of the dissimilar Al/Mg joint by the UTS of the BM (Mg). At constant tool rotation speed, the FS welded joints exhibited a weak joint efficiency of approximately between 18% and 27% (see Fig. 11(a)) showing that

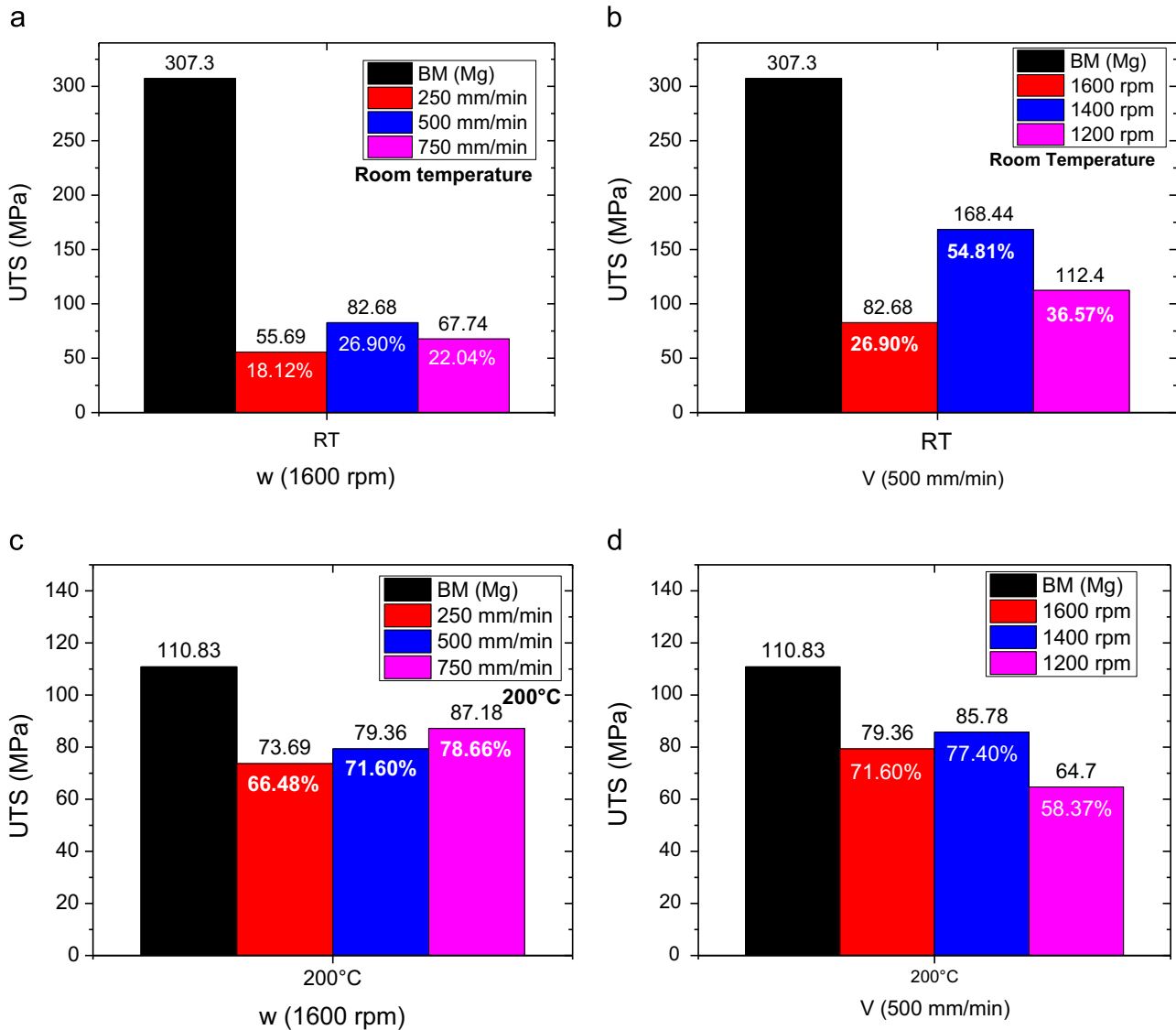


Fig. 11. Ultimate tensile strength (UTS) calculated at different tool rotation speed and tool translation speed (a) and (b) at room temperature, (c) and (d) at 200 °C, respectively.

the maximum joint efficiency was obtained at 500 mm/min tool translation speed. Fig. 11(b) presents the ultimate tensile strength of joints obtained at constant tool translation speed and tool rotation speeds of 1200 rpm, 1400 rpm, and 1600 rpm. The joint efficiency was ranging between 27% and 55% with the higher value obtained at 1400 rpm rotation speed.

3.3.2. High temperature

The engineering stress–strain response of uniaxial tensile tests conducted at 200 °C of dissimilar butt welded Al/Mg joints with Al in the AS obtained using constant rotational speed (1600 rpm), is presented in Fig. 9(c). It can be noticed that using tool translation speed of 750 mm/min resulted in higher strain to failure compared to the specimen obtained using 250 mm/min or 500 mm/min. The tool translation speed of 750 mm/min is observed to present the optimum mechanical properties at elevated temperatures compared to the two other weld conditions. Fig. 9(d) presents the tensile stress–strain curves at 200 °C of Al/Mg joints obtained using constant tool translation speed (500 mm/min) and varying tool rotational speed. It is observed that using 1400 rpm tool rotation speed resulted in the highest tensile strength and strain to failure. The joint efficiency of the welds at 200 °C were calculated,

and the results were presented in Fig. 11. Under constant tool rotational speed of 1600 rpm (Fig. 11(c)), an improvement of the joint efficiency at 200 °C is evident compared to room temperature and the values were found to be between 66 and 79%. The joint efficiency is observed to increase with increasing tool translation speed to reach its maximum value at 750 mm/min. In the case of constant translation speed (500 mm/min) the joint efficiency reached a maximum value of approximately 77% using 1400 rpm tool rotation speed, as shown in Fig. 11(d).

3.4. Fractography

In order to visually investigate the Al-to-Mg FS welded joint specimen failure, a tensile test specimen was ground up to 1200 grit SiC polishing paper. Images were obtained after tensile testing to observe the failure characteristics of the welded joint. Fig. 12 presents a specimen failed under tensile test with the joint being prepared using 1400 rpm tool rotational speed and 500 mm/min tool translation speed with Al on the AS. Fig. 12(a) and (b) are observation of the failed specimen in the ND–TD plane. It can be observed from that the failure occurred along the line of the joint, between aluminum and magnesium. Moreover, the fracture seems

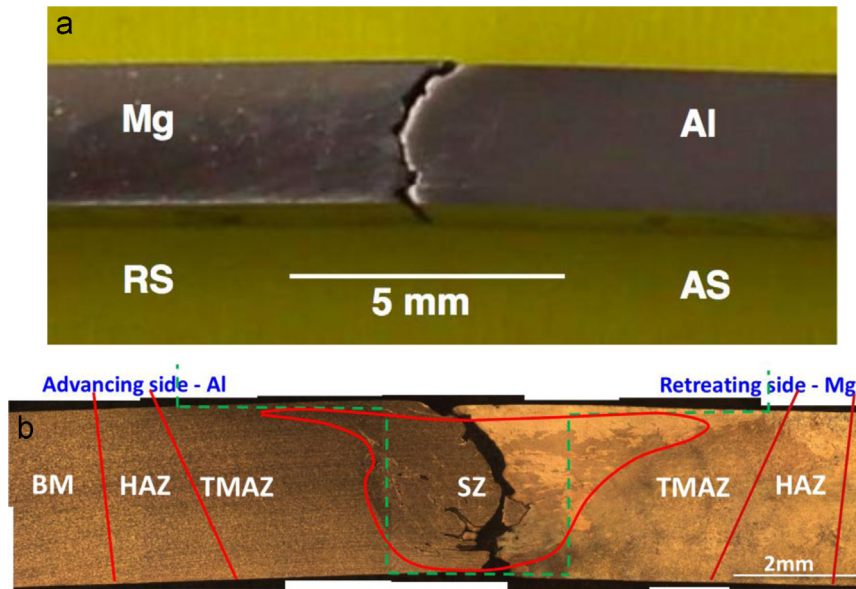


Fig. 12. Dissimilar FS welded specimen using 1400 rpm and 500 mm/min fractured after tensile loading, (a) macroscopic observation (b) etched specimen observed with optical microscope.

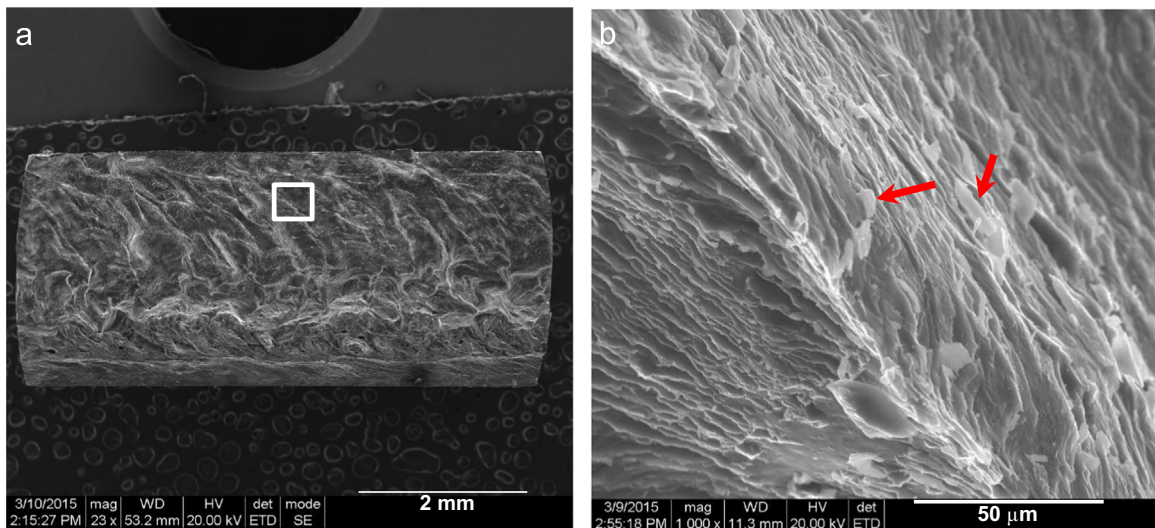


Fig. 13. SEM fractography of an FS welded sample using 1400 rpm and 500 mm/min at room temperature.

to have initiated in the IMCs forming the interface between aluminum and magnesium. Furthermore, the cracks seem to have occurred along the interface between the aluminum and the IMCs, as we can observe aluminum fractions in the magnesium part of the weld. These results are in correlation with the observations in Fig. 8, precisely, the peak in the microhardness values in the SZ and the variation of the percentage of IMCs in the aluminum side. Dorbane et al. reported that at temperature lower or equal to 200 °C the main crack initiation mechanism in Al 6061 T6 is particles fracture which also presented lower ductility compared to AZ31B Mg [33]. Moreover, the IMCs have a brittle behavior; with dislocations accumulating at the interface with aluminum or magnesium, the IMCs will develop cracks. In the purpose of bringing further insight on the crack initiation mechanism, the fractured surface on the magnesium side of a specimen tensile tested at room temperature, prepared using 1400 rpm and 500 mm/min weld parameters is shown in Fig. 13. Fig. 13 (a) presents chevron patterns on the fractured surface, which is

characteristic of a brittle fracture. Fig. 13(b) presents a magnified region of the upper zone of the fractured surface showing ridges and broken IMCs. From the previous observation, we can suppose that the cracks are initiating either in the IMCs formed at the interface between the aluminum and the magnesium parts, or by debonding of the interface between the IMCs and the aluminum part.

4. Conclusions

The following conclusions can be made based on the present study on friction stir welding on dissimilar metals – aluminum and magnesium:

- AZ31B magnesium alloy was successfully FS welded with 6061-T6 aluminum alloy with different parameters and material configurations.

- The examination of the FS welded joints cross section area, having aluminum on advancing side of the FSW resulted in better welds with fewer defects in the stir zone.
- Among the studied weld process parameters, 1400 rpm rotational speed and 500 mm/min translational speed resulted in the optimum joint quality, based on the analysis of the weld integrity and microstructure. The optimum parameters obtained in the study were found for the particular tool geometry used in the present work.
- Both Mg-rich and Al-rich sides of the stir zone revealed grain refinement, with the SZ grain sizes reducing to $2.43 \pm 0.87 \mu\text{m}$ and $0.94 \pm 0.24 \mu\text{m}$ on the Mg and Al sides, respectively.
- A thin layer of intermetallic compounds (IMC) were observed in the stir zone at the interface between the welded sheets, which affected the weld properties.
- The microhardness showed a lower hardness values (55–65 HV) in the magnesium base material and higher values (120–135 HV) in aluminum base material, with a transition in the stir zone and some peaks due to the IMCs in the SZ.
- Uniaxial tensile testing were performed at different temperatures, the strength of the joint was influenced by both FSW parameters and tensile testing temperature. Room temperature joint efficiency of the welds prepared in the current study were between 18% and 55% while at elevated temperature the joint efficiency were between 58% and 79% for the different parameters.
- Brittle fracture was observed on the specimens tested under tensile loading, with the fracture surface showing chevron pattern. The specimens have fractured along the welded joint with the fracture initiating in the IMCs between the Al and Mg.

Acknowledgment

The authors acknowledge the support provided by Qatar National Research Fund under NPRP Grant # 4-1063-2-397 for this work. QNRF is a constituent member of the Qatar Foundation.

References

- [1] T.M. Pollock, Weight loss with magnesium alloys, *Science* 328 (2010) 986–987.
- [2] S.N. Mathaudhu, E.A. Nyberg, Magnesium alloys in U.S. military applications: Past, current and future solutions, in: S.R. Agnew, R. NN, A. NE, H. SW (Eds.), *Magnesium Technology*, 2010, pp. 27–32.
- [3] P. Liu, Y. Li, H. Geng, J. Wang, Microstructure characteristics in TIG welded joint of Mg/Al dissimilar materials, *Mater. Lett.* 61 (2007) 1288–1291.
- [4] A. Ben-Artzy, A. Munitz, G. Kohn, B. Bronfin, A. Shtechman, Joining of light hybrid constructions made of magnesium and aluminum alloys, *TMS Annual Meeting*, 2002, pp. 295–302.
- [5] C.-T. Chi, C.-G. Chao, T.-F. Liu, C.-H. Lee, Aluminum element effect for electron beam welding of similar and dissimilar magnesium–aluminum–zinc alloys, *Scr. Mater.* 56 (2007) 733–736.
- [6] S. Bannour, K. Abderrazak, S. Mattei, J.E. Masse, M. Autric, H. Mhiri, The influence of position in overlap joints of Mg and Al alloys on microstructure and hardness of laser welds, *J. Laser Appl.* 25 (2013) 032001.
- [7] L. Liu, D. Ren, F. Liu, A review of dissimilar welding techniques for magnesium alloys to aluminum alloys, *Materials* 7 (2014) 3735–3757.
- [8] L. Liu, J. Tan, X. Liu, Reactive brazing of Al alloy to Mg alloy using zinc-based brazing alloy, *Mater. Lett.* 61 (2007) 2373–2377.
- [9] Z. Wang, H. Wang, L. Liu, Study on low temperature brazing of magnesium alloy to aluminum alloy using Sn–xZn solders, *Mater. Des.* 39 (2012) 14–19.
- [10] L.M. Zhao, Z.D. Zhang, Effect of Zn alloy interlayer on interface microstructure and strength of diffusion-bonded Mg–Al joints, *Scr. Mater.* 58 (2008) 283–286.
- [11] L.M. Liu, L.M. Zhao, R.Z. Xu, Effect of interlayer composition on the microstructure and strength of diffusion bonded Mg/Al joint, *Mater. Des.* 30 (2009) 4548–4551.
- [12] J. Shang, K. Wang, Q. Zhou, D. Zhang, J. Huang, G. Li, Microstructure characteristics and mechanical properties of cold metal transfer welding Mg/Al dissimilar metals, *Mater. Des.* 34 (2012) 559–565.
- [13] J. Wang, J. Feng, Y. Wang, Microstructure of Al–Mg dissimilar weld made by cold metal transfer MIG welding, *Mater. Sci. Technol.* 24 (2008) 827–831.
- [14] P. Xue, B.L. Xiao, Q. Zhang, Z.Y. Ma, Achieving friction stir welded pure copper joints with nearly equal strength to the parent metal via additional rapid cooling, *Scr. Mater.* 64 (2011) 1051–1054.
- [15] F. Liu, D. Ren, L. Liu, Effect of Al foils interlayer on microstructures and mechanical properties of Mg–Al butt joints welded by gas tungsten arc welding filling with Zn filler metal, *Mater. Des.* 46 (2013) 419–425.
- [16] F. Liu, Z. Zhang, L. Liu, Microstructure evolution of Al/Mg butt joints welded by gas tungsten arc with Zn filler metal, *Mater. Charact.* 69 (2012) 84–89.
- [17] A. Panteli, J.D. Robson, I. Brough, P.B. Prangnell, The effect of high strain rate deformation on intermetallic reaction during ultrasonic welding aluminium to magnesium, *Mater. Sci. Eng. A* 556 (2012) 31–42.
- [18] J. Robson, A. Panteli, P.B. Prangnell, Modelling intermetallic phase formation in dissimilar metal ultrasonic welding of aluminium and magnesium alloys, *Sci. Technol. Weld. Join.* 17 (2012) 447–453.
- [19] F. Hayat, The effects of the welding current on heat input, nugget geometry, and the mechanical and fractural properties of resistance spot welding on Mg/Al dissimilar materials, *Mater. Des.* 32 (2011) 2476–2484.
- [20] I. Bhamji, M. Preuss, R. Moat, P. Threadgill, A. Addison, Linear friction welding of aluminium to magnesium, *Sci. Technol. Weld. Join.* 17 (2012) 368–374.
- [21] M.A. Mofid, A. Abdollah-Zadeh, F.M. Ghaini, C.H. Gur, Submerged friction-stir welding (SFSW) underwater and under liquid nitrogen: An improved method to join Al alloys to Mg alloys, *Metall. Mater. Trans. A* 43 (2012) 5106–5114.
- [22] T. Morishige, A. Kawaguchi, M. Tsujikawa, M. Hino, T. Hirata, K. Higashi, Dissimilar welding of Al and Mg alloys by FSW, *Mater. Trans.* 49 (2008) 1129–1131.
- [23] X. Cao, C. Garnier, P. Wanjara, Tensile strength of friction stir spot welded dissimilar AA5754-to-AZ31B alloys, in: *Proceedings of the 9th International Conference on Trends in Welding Research*, June 4, 2012 - June 8, 2012, Chicago, IL, ASM International, United states, 2013, pp. 572–579.
- [24] R. Zettler, J.F. Dos Santos, A. Blanco, A. Da Silva, A study on dissimilar friction stir welds between Al and Mg alloys, in: *Proceedings of the 7th International Conference on Trends in Welding Research* May 16, 2005 - May 20, 2005, ASM International Pine Mountain, GA, United states, 2005, pp. 413–419.
- [25] M. Cabibbo, D. Ciccirelli, A. Di Salvia, G. Quercetti, S. Spigarelli, Microstructural aspects of a friction stir welded joint of magnesium AZ31 and aluminium 6060 alloys, *Metall. Ital.* 1 (2012) 13–18.
- [26] F. Hunt, Q. Yang, H. Badarinarayan, K. Okamoto, D. Platt, Friction stir welding of dissimilar magnesium alloys for automotive applications, *2007 World Congress April 16, 2007–April 19, 2007*, SAE International Detroit, MI, United States, 2007.
- [27] R. Zettler, A.A.M. da Silva, S. Rodrigues, A. Blanco, J.F. dos Santos, Dissimilar Al to Mg alloy friction stir welds, *Adv. Eng. Mater.* 8 (2006) 415–421.
- [28] V. Firouzidor, S. Kou, Al-to-mg friction stir welding: effect of material position, travel speed, and rotation speed, *Metall. Mater. Trans. A* 41 (2010) 2914–2935.
- [29] S. Malarvizhi, V. Balasubramanian, Influences of tool shoulder diameter to plate thickness ratio (D/T) on stir zone formation and tensile properties of friction stir welded dissimilar joints of AA6061 aluminum–AZ31B magnesium alloys, *Mater. Des.* 40 (2012) 453–460.
- [30] Y.S. Sato, S.H.C. Park, M. Michiuchi, H. Kokawa, Constitutional liquation during dissimilar friction stir welding of Al and Mg alloys, *Scr. Mater.* 50 (2004) 1233–1236.
- [31] R.S. Mishra, P.S. De, N. Kumar, *Friction stir welding and processing*, Springer International Publishing, Switzerland, 2014.
- [32] R.S. Mishra, Z.Y. Ma, Friction stir welding and processing, *Mater. Sci. Eng. R* 50 (2005) 1–78.
- [33] A. Dorbane, G. Ayoub, B. Mansoor, R. Hamade, G. Kridli, A. Imad, Observations of the mechanical response and evolution of damage of AA 6061-T6 under different strain rates and temperatures, *Mater. Sci. Eng. A* 624 (2015) 239–249.
- [34] B. Mansoor, A. Dorbane, G. Ayoub, A. Imad, Friction stir welding of AZ31B magnesium alloy with 6061-T6 aluminum alloy: Influence of processing parameters on microstructure and mechanical properties, in: R.S. Mishra, M. W. Mahoney, Y. Sato, Y. Hovanski (Eds.), *Friction Stir Welding and Processing VIII - The Minerals, Metals and Materials Society*, 2015, pp. 259–266.
- [35] Y. Morisada, T. Imaizumi, H. Fujii, Determination of strain rate in friction stir welding by three-dimensional visualization of material flow using X-ray radiography, *Scr. Mater.* 106 (2015) 57–60.
- [36] N. Kumar, R.S. Mishra, C.S. Huskamp, K.K. Sankaran, The effect of friction stir processing on the microstructure and mechanical properties of equal channel angular pressed 5052Al alloy sheet, *J. Mater. Sci.* 46 (2011) 5527–5533.
- [37] V. Firouzidor, S. Kou, Formation of liquid and intermetallics in Al-to-Mg friction stir welding, *Metall. Mater. Trans. A* 41 (2010) 3238–3251.
- [38] Z. Liang, K. Chen, X. Wang, J. Yao, Q. Yang, L. Zhang, A. Shan, Effect of tool offset and tool rotational speed on enhancing mechanical property of Al/Mg dissimilar FSW joints, *Metall. Mater. Trans. A* 44 (2013) 3721–3731.
- [39] J. Mohammadi, Y. Behnamian, A. Mostafaei, H. Izadi, T. Saeidi, A.H. Kokabi, A. P. Gerlich, Friction stir welding joint of dissimilar materials between AZ31B magnesium and 6061 aluminum alloys: microstructure studies and mechanical characterizations, *Mater. Charact.* 101 (2015) 189–207.
- [40] B. Fu, G. Qin, F. Li, X. Meng, J. Zhang, C. Wu, Friction stir welding process of dissimilar metals of 6061-T6 aluminum alloy to AZ31B magnesium alloy, *J. Mater. Process. Technol.* 218 (2015) 38–47.
- [41] A. Masoudian, A. Tahaei, A. Shakiba, F. Sharifianjazi, J.A. Mohandesi, Microstructure and mechanical properties of friction stir weld of dissimilar AZ31-O magnesium alloy to 6061-T6 aluminum alloy, *Trans. Nonferrous Met. Soc. China* 24 (2014) 1317–1322.
- [42] S. Samson, The crystal structure of the phase [beta] Mg₂Al₃, *Acta Crystallogr.* 19 (1965) 401–413.

- [43] M.X. Zhang, H. Huang, K. Spencer, Y.N. Shi, Nanomechanics of Mg–Al inter-metallic compounds, *Surf. Coat. Technol.* 204 (2010) 2118–2122.
- [44] Chen Gq, Shi Qy, Li Yj, Sun Yj, Dai Qi, Jia Jy, Zhu Yc, Wu Jj, Computational fluid dynamics studies on heat generation during friction stir welding of aluminum alloy, *Comput. Mater. Sci.* 79 (2013) 540–546.
- [45] A.H. Ammouri, G. Kridli, G. Ayoub, R.F. Hamade, Relating grain size to the Zener–Hollomon parameter for twin-roll-cast AZ31B alloy refined by friction stir processing, *J. Mater. Process. Technol.* 222 (2015) 301–306.
- [46] L. Commin, M. Dumont, J.E. Masse, L. Barrallier, Friction stir welding of AZ31 magnesium alloy rolled sheets: Influence of processing parameters, *Acta Mater.* 57 (2009) 326–334.
- [47] J.P. Young, H. Askari, Y. Hovanski, M.J. Heiden, D.P. Field, Thermal microstructural stability of AZ31 magnesium after severe plastic deformation, *Mater. Charact.* 101 (2015) 9–19.
- [48] A.N. Albakri, B. Mansoor, H. Nassar, M.K. Khraisheh, Thermo-mechanical and metallurgical aspects in friction stir processing of AZ31 Mg alloy—a numerical and experimental investigation, *J. Mater. Process. Technol.* 213 (2013) 279–290.
- [49] V. Firouzdor, S. Kou, Al-to-Mg friction stir welding: Effect of positions of Al and Mg with respect to the welding tool, *Weld. J.* 88 (2009) 213–224.
- [50] K.-J. Lee, E.-P. Kwon, Microstructure of stir zone in dissimilar friction stir welds of AA6061-T6 and AZ31 alloy sheets, *Trans. Nonferr. Met. Soc. China* 24 (2014) 2374–2379.
- [51] A. Somasekharan, L. Murr, Microstructures in friction-stir welded dissimilar magnesium alloys and magnesium alloys to 6061-T6 aluminum alloy, *Mater. Charact.* 52 (2004) 49–64.